Highly Sensitive Composite Foam Bodily Sensors Based on G-Putty Ink Soaking Procedure

Conor S Boland*[1], Daniel P O'Driscoll[2,3], Adam G Kelly[2,3], John B Boland[2,3] and Jonathan N Coleman[2,3]

[1]*School of Mathematical and Physical Sciences, University of Sussex, Brighton, BN1 9QH, U.K.*
[2]*School of Physics, Trinity College Dublin, Dublin 2, Ireland*
[3]*CRANN & AMBER Research Centers, Trinity College Dublin, Dublin 2, Ireland*

*c.s.boland@sussex.ac.uk (Conor S. Boland)

KEYWORDS
graphene, ink, composite, foam, strain sensing, bodily sensing, smart materials, pulse

ABSTRACT
Electrically conductive composite materials are highlighted as a potential tech path towards future flexible devices for wearable health technologies. To be commercially viable, these materials must not only be mechanically soft, highly sensitive to deformation and report a sustainable signal but also utilise manufacturing methods that facilitate large scale production. An ideal candidate for these envisioned technologies is the viscous, electromechanically sensitive composite material g-putty. Inks based off of g-putty here are shown to transform a commercial polymer foam into a sensitive strain sensing material through a simple, scalable soaking procedure. Foam composites reported here have sensitives as high as ~20 in terms of compressive strain and ~0.4 kPa^{-1} with respect to applied compressive stress; both values being comparable to the parent g-putty material. Through g-putty's self-adhering nature, the foams used acted as an elastic scaffolding that aided in overcoming many of the hysteresis effects associated with g-putty without the need to further encapsulation methods. From this, these composite foams were demonstrated to have a sustainable signal which allowed for effective impact and vital sign sensing.

INTRODUCTION

Electromechanically sensitive nanocomposites are an exciting and ever expanding subsection of material science. The functionality of these materials are based on the simple principle of applied deformation results in a bulk piezoresistive response.[1, 2] Most commonly, these materials are formed through the mixing or deposition of one and two-dimensional nanomaterials into/onto soft elastomeric polymers.[2-4] In application, these materials are envisioned as the future of medical diagnostics due to their high sensitivity to strain,[5, 6] compliant nature[7, 8] and ability to be scalably produced.[9, 10] Composite sensor research so far has successfully demonstrated a variety of these materials in potentially commercialisable real-time bodily movement and vital sign measurement applications.[11] At the forefront, g-putty is one of the most unique prospects in realising the goal of nanocomposite sensors reaching the marketplace.[12] G-putty, is a mixture of graphene and home-made "*Silly Putty*", a novelty material made of polysiloxane lightly cross-linked with boric acid.[13, 14] With unparalleled sensitivity, scalability, and viscous nature, g-putty has been demonstrated to be one of the most highly accurate bodily sensors in literature.[12, 13] On average, a nanocomposite's sensitivity is ~40[11] but in comparison g-putty far surpasses its competitors by displaying sensitives >500.[13] Furthermore, with a Young's modulus of ~200 kPa, g-putty presents mechanical properties that better facilitate application for skin-on sensing with respect to other nanocomposite materials that on average have moduli of ~300 MPa.[11] Currently, a sensing material that combines high sensitives, low mechanical properties and a sustainable signal is an unmet need. With its current properties, g-putty would be the ideal candidate.

However, despite such a large amount of potential upside, g-putty still comes with intrinsic material drawbacks. At strains >2%, g-putty displays a highly viscoplastic nature, an inherent property of the silly putty matrix.[12] For application at larger strains, such as repeated joint or impact sensing, permanent deformation is problematic as it can lead to signal dampening and drift. Furthermore, electronically, the graphene nanofiller network in g-putty displays dynamic percolation at room temperature resulting in flake mobility inside the viscous polymer matrix.[13] This flake movement manifests itself as a bulk resistive decay, with nanosheets relaxing into lower energy states with respect to time. Though not insurmountable with signal processing, it would require additional electronic components to be overcome in any future applications.

Here, we resolve all the above stated issues with g-putty without compromising any of material's electromechanical sensitivity and meet all the previously detailed requirements for

commercial application. By creating composite inks from bulk g-putty, it was demonstrated that soft commercial foams soaked in the inks can act as an elastic scaffold, stabilising the deposited material. Interestingly, the electromechanical signal drift associated with g-putty was found to be non-existent and the reported electromechanical sensitivity unperturbed by the soaking process. The advantage of using foam substrates was that they are already manufactured on a large scale and are widely applied in commercial apparel. Also, by utilising simple solution processing techniques to create and incorporate our inks into the foam structure we demonstrate a process that can be seamlessly integrated into commercial foam production.[1] These smart foams can be easily made into any desired dimension and then introduced into or replace current foam materials in apparel to create next generation smart biomonitoring clothing. One example of an unmet need in the market are the accurate measurement of impacts to the body of an athlete for injury prevention.[15] By replacing the foams found in the protective undergarments or shoe insoles of athletes with the materials here, it would enable the measurement of impacts experienced by the wearer in real-time during athletic activities and allow for the retroactive evaluation of performance.[16]

RESULTS AND DISCUSSION

Characterising Bulk G-putty

Defect free, liquid phase exfoliated graphene was produced through the tip sonication of graphite in *N*-methyl-pyrrolidone.[17] The liquid was size selected through centrifugation, filtered and redispersed in chloroform to form a stock solution (see Methods in Supporting Information). In Figure 1A, a representative Transmission Electron Microscopy (TEM) imagine of the resultant processed nanosheets can be seen. All flakes are found to be large, few layer, and electron transparent. Statistics taken from TEM (Figure 1B) show that the flakes are on average ~500 nm in length and are 1-6 monolayers thick.[18] Using the authors previously developed optimised silly putty production protocol,[14] pristine putty was made and then formed into an 8.5 vol% g-putty sample by mixing the putty with the stock graphene solution (inset Figure 1B). This loading level was chosen as it is reported to be near the percolation threshold of the material where electromechanical properties will be maximised.[13] As previously stated, g-putty suffers from two intrinsic material draw backs, a decay in resistance with time and plastic deformation above 2% strain. In Figure S1A, the characteristic decay in bulk resistance as a function of time at 0% strain was seen, with resistance decreasing by a factor of ~2.5 in ~500s. To examine the level of plasticity of the material, hysteresis testing up to 40% strain were performed in both tension (Figure 1C) and compression (Figure 1D) on the g-putty sample over eight strain steps. In both cases, g-putty displayed very large hysteresis

loops above 2% strain and showed no sign of mechanical recovery. During this strain cycling regime, the g-putty sample was clearly seen to plastically deform inside the sample holding clamps (Figure E). To quantify the performance quality of the g-putty material produced, tensile and compressive electromechanical testing was performed in Figures 1F-G. The standard metric in which the electromechanical performances of materials are compared, the Gauge Factor (*G*), can be described in two ways. Firstly by[19]

$$\frac{\Delta R}{R_0} = \frac{1}{\rho_{0,\varepsilon}} \frac{d\rho(\varepsilon)}{d\varepsilon} + 2 = G_\varepsilon \varepsilon \quad (1)$$

Where ε is either tensile or compressive strain, $\rho(\varepsilon)$ is the resistivity with applied strain, $\rho_{0,\varepsilon}$ the zero-strain resistivity, G_ε is the gauge factor with respect to strain and $\Delta R/R_0$ is the fractional resistance change. For traditional metal-based strain sensors, which exhibit resistivity independent behaviour, values of G_ε in tension are expected to be ~2.[19] However for g-putty, this figure of merit in tension can be as high as ~1000[13] due to network and tunnelling effects leading to large changes in the resistivity of the nanofiller network. Alternatively, a materials sensitivity to applied compressive stress can be similarly described as[20]

$$\frac{\Delta R}{R_0} = \frac{1}{\rho_{0,\sigma}} \frac{d\rho(\sigma)}{d\sigma} + 2 = G_\sigma \sigma \quad (2)$$

Where σ is stress in units of kPa, $\rho(\sigma)$ is the resistivity with applied stress, $\rho_{0,\sigma}$ the zero-stress resistivity, and G_σ is the gauge factor with respect to stress in units of kPa^{-1}. On average for a composite material the value for G_σ in compressive testing generally is found to range from 0.02 to 6 kPa^{-1}.[1, 20] The stock g-putty here was reported to have values for G_ε in tension and G_σ in compression of ~238 and ~0.24 kPa^{-1} respectively. These values are in keeping with previously reported values for g-putty of a similar loading level.[13] In Figure 1H, the effects of hysteresis on the stability of g-putty's electromechanical signal under cycling loading is reflected in compressive cyclic testing undergone between 5 and 30% strain at 100 mm min^{-1} for 500 cycles (Figure S1B for full cycle range). When comparing the electrical output in resistance (red) to the driving strain profile (black), a clear desync was seen in the signal. For comparison, in Figure S4C and D, compressive

cyclic tests performed between 0.2 to 1% strain, below the hysteresis threshold, reported no signal drift. From the characterisation of the stock g-putty sample the material has excellent strain sensing performances however, there are clear material obstacles that must be overcome to realise g-putty's full potential in application.

Characterising Foams Soaked in G-putty Ink

We believe that the above mentioned material obstacles can be overcome through the creation and application of inks formulated from bulk g-putty. In the author's previous work, we demonstrated that g-putty can be dissolved in common solvents to form inks with long term stability (Figure S2A).[12] From these inks, g-putty can be reconstituted through a variety of ink printing methods into patterned heterostructures on flexible substrates. The hypothesis here is that by soaking a commercial foam in g-putty ink, the foam would act as an elastic scaffolding for which g-putty could adhere to and be mechanically stabilised by. Using the principles from a previous study where the author's developed a soaking method for commercial foams in graphene dispersions,[20] foams were cut into the desired dimensions and washed to remove containments (see Methods in Supporting Information). After which, the pieces of foams were soaked in chloroform-based g-putty inks of different concentration and dried to form composite foams ranging in mass fraction (M_f) from 0 to 40%. Soaking resulted in the foams changing from a light cream colour to a grey/black hue, characteristic of graphene composites (Figure 2A). Scanning Electron Microscopy (SEM) images of the pristine and M_f ~7.5% foam in Figures 2B and C respectively showed that the interior porous structure of the foam was unaffected by the g-putty coating. Close-ups of the coating in Figure 2D show the internal structure of the foam to be evenly coated, with graphene flakes being very prominently shown and no apparent sign of a polymer coating. Comparing the Raman spectra of a (top to bottom) M_f ~7.5% composite foam, g-putty, pristine putty and pristine commercial foam in Figure 2E, the graphene signal with all the characteristic bands was found to dominate the spectra of the composite.[13] Distinct bands associated with the pristine foam and putty materials however can still be faintly seen within the spectra of the composite at Raman shifts of ~2900 cm^{-1}. However, as these bands occur at similar Raman shifts due to both materials being polysilicone-based, they are indistinguishable. Most notable from Raman is that the quality of the graphene material in the composite foams was unaffected by the g-putty ink soaking process, with no notable changes in band intensity ratios[21] nor were morphological changes noted in follow-up TEM on the inks themselves (Figure S2B).

Electronic Properties

Looking at the electrical properties of the composites, the once insulating pristine foam was reported to become electrically conductive upon the introduction of critical loadings of g-putty through soaking. Plotting conductivity as a function of M_f in Figure 3A, conductivity was found to increase from ~10^{-7} S/m at M_f ~7.5% to ~10^{-3} S/m at M_f ~40%. Like many conductive composite materials, the increase in conductivity (γ) with loading level of conductive filler can be described using percolation theory and fitted with the following power law[22]

$$\gamma = \gamma_f(\varphi_f - \varphi_0)^t \quad (3)$$

Where φ_c is the loading level at which the first conductive pathway across the composite forms (*i.e.* the percolation threshold), φ_f is the loading level in M_f and γ_f and t are constants. For 3-dimension transport of charge, t typically has a value of ~2.[22] Fitting Eq 3 to Figure 3A (solid line), values for φ_c and t are found to be ~7.2% and ~2.4 respectively. However, this increase in conductivity with loading level could be considered counterintuitive. When considering this particular system, a coating with a well-defined conductivity is being introduced onto a scaffold structure. Thus, seeing percolation-like scaling that saturates above the bulk coatings conductivity would not be expected. This scaling however is consistent with the author's previous work on g-putty inks.

During the deposition and drying of g-putty inks during printing, it was reported that there is a large shift in network morphology from polydispersed to a segregated system.[12] This was made possible by the viscous nature of the putty matrix and was a manifestation of dynamic percolation accelerated by a decrease in matrix viscosity due to the presence of the solvent used to form the ink. The resultant is a heterostructure where a large population of the graphene nanosheets reside on top of a putty layer. This varying degree of phase separation brought about by these ink drying effects led to large changes in electrical conductivity, with spray coated samples showing a 6 order of magnitude increase in conductivity over the bulk form of similar loading level.[12] Despite this phase separation, printed materials based off g-putty inks kept their bulk properties and reported values of G_ε in tension >100, similar to the bulk material used for ink formulation.[12] We believe that the above mentioned phenomena is consistent with this unexpected percolation-like behaviour in Figure 3A. As inks with various concentrations are being applied in this work, it would result in different densities of graphene in the top layer of

the phase separated coating. Reflecting on the SEM images and the percolation exponent of the foam system, all are consistent with a graphene layer with very little polymer coating on the nanosheet surfaces or at the nanosheet junctions.[23] However, in a comparative graphene coated polyurethane foam system, an electrical conductivity of ~10^{-5} S/m is reported at a percolation threshold of M_f ~0.75%.[20] These values respectively are two orders of magnitude higher and one order of magnitude lower than what is reported for the foams here. Thus, the presence of the putty under layer still greatly influences current conduction in the composites despite not being well observable.

Mechanical Properties

To examine the mechanical properties of the composite foams, the materials were subjected to compressive mechanical testing (Figure 3B-D,S3). In Figure 3B, the introduction of the g-putty coating gradually increased the mechanical properties of the foam materials up until M_f ~ 8% (representative stress-strain curves can be found in Figure S3A). After which all values plateau and were found to scatter around a somewhat constant value. This saturation point for the mechanical properties is noted to be quite similar to the electrical percolation threshold. The Max Stress (σ_{max}), Young's modulus (Y) and Toughness (T) of the foams in this initial value range were found to increase from ~56 kPa, ~27 kPa and ~87 kJ/m^3 respectively to the corresponding values of ~114 kPa, ~44 kPa and ~150 kJ/m^3 at the M_f saturation point. Relative to other composite materials applied as strains sensors, from a recent study, the modulus values here are less than ~77% of reported literary values.[11] Noted in this same study, values of Young's modulus <300 kPa (*i.e.* the modulus of human skin) greatly enhance a materials prospects of application as a wearable material for bodily monitoring in regards to signal clarity and the wear's comfort. Here, we report our materials to be far below this application threshold, even at the highest tested loading level. In terms of hysteresis, the composite foams display curves comparable to that of the pristine foam (Figures 3C and D, S3B and C). When comparing the pristine foam in Figure 3C and a M_f ~ 30% foam in Figure 3D, it was noted there is minimal change in the loop size even with such a high loading level.

Electromechanical Properties

In relation to the composite's electrical properties as a function of time, the composite foams show no sign of the resistive decay that was observed in bulk g-putty. When held at 0% strain for a period of ~450s (Figure S4), a M_f ~ 7.5% foam presented a constant resistance signal with

respect to time. Looking at the electromechanical response of the composites in Figures 4A-D, S5A-D as a function of loading level, the foams showed an expected changed in electrical resistance as a function of applied strain and stress. For all plots, $\Delta R/R_0$ was found to initially increase linearly until a critical strain/stress value of ~17% and ~7 kPa respectively. These critical values are noted to be similar across all loading levels (Figure S4E) and closely match values for the yield strain and stress of the composites. These critical values run some parallels with the electromechanical performance metric the Working Factor, which describes the strain limit of a material's linear electromechanical response and corresponds to the yield point.[11] Beyond these critical values, $\Delta R/R_0$ decreased due to a combination of effects caused by geometric changes that resulted in the internal pore structure of the foam to collapse with applied deformation resulting in nanosheets becoming more well connected and the electrode distance decreasing. The shape of electromechanical response curves here resembles closely what was reported in a similar graphene coated foam system.[20] To note, the presence of the critical strain/stress would imply that the composites here can function effectively as highly sensitive low strain/stress sensing materials.

In Figure 4A, $\Delta R/R_0$ vs strain for a select range of M_f was shown. Plotting these curves on a log-log plot (Figure 4B), a clear linear region at low strain was observed in accordance with Eq 1. All data (Figures 4B, S5B) was reported to reside above a value of $G_\varepsilon \sim 2$ (dashed line). Similarly, in Figures 4C and D, $\Delta R/R_0$ vs stress presented the same linear behaviour at low stress and using Eq 2, all data (Figures 4D, S5D) were found to reside above $G_\varepsilon \sim 0.01$ kPa^{-1} (dashed line). Plotting the extrapolated values for G_ε and G_σ as a function of M_f and electrical conductivity (Figure 4E and F), each metric was found to decrease from ~11 and ~0.3 kPa^{-1} at M_f ~7.5% and ~10^{-7} S/m to ~2 and ~0.03 kPa^{-1} at M_f ~40% and ~10^{-3} S/m respectively. In comparison to a broad range of strain sensing systems applying a range of nanomaterial and polymer type, values of G reported here were found to be larger than more than half of nanocomposites materials sampled in a study on 200 sensing systems.[11] This trend in the sensitivity with M_f is characteristic of most nanocomposite systems, where gauge factor peaks around electrical percolation and then diminishes with increasing loading level, and thus electrical conductivity, due to an increase in connectivity of the nanofiller network.[24 25] The manner in which the sensitivity metrics decreases in the data here however gives rise to some interesting scaling. In Figure 4E gauge factor scales inversely with M_f, denoted by the solid line overlaying the data. This trend was noted to be similar to scaling in tensile G_ε reported in spray coated g-putty inks up until at sensitivity saturation point of M_f ~11%.[12] Additionally in

Figure 4F, gauge factor was found to scale as the cubed root of electrical conductivity (solid line). This again was a behaviour noted by the authors in previous works on bulk and ink-based g-putty and maybe a manifestation of percolation and tunnelling effects.[12, 14]

In comparison to bulk g-putty, the sensitivity metrics for the foam materials have maximum values that match quite closely that of the bulk. This means that the soaking process had no effect on the compressive electromechanical performance of g-putty. With respect to other foam sensor materials, similarly structured graphene coated polymer foams were reported to have sensitives of G_ε ~ 4 and G_σ ~ 0.05 kPa^{-1}.[20] An rGO free standing foam reported a slightly higher value for G_ε of ~12.5.[26] For a reduced graphene oxide foam coated in PDMS, G_σ was reported to be ~0.01 kPa^{-1}.[25] To further understand the electromechanical properties of the composites foams, the tensile response of a M_f ~7.5% composite foam with a longer length (~4cm) but with the same cross-sectional area was examined (Figure S6A). This material however was found to have a tensile G_ε of ~10, much lower than the value of ~238 previously seen for the bulk material. Thus, in application compressive conditions would be more desirable. However, to verify that this longer sample was still of good quality and that the measurement was not an artifact of poor production due to increased sample length, electromechanical compression tests were also performed on the sample. A value of G_σ ~0.4 kPa^{-1} was recorded (Figure S6B)

Signal Stability

To compare directly the improvements in performance between the bulk g-putty and its composite foam form, a M_f ~ 7.5% (the most sensitive loading level) was selected. Step strain testing was performed on the two materials where by a compressive strain of 2% was applied and then held. Under these conditions, g-putty's displayed its large resistive decay, with resistance falling by a factor of 5 after ~600s (Figure S7A). However, the composite foam displayed an improved performance, with resistance relaxing slightly by a factor of ~1.1 over the initial few seconds of test time after which it remains unperturbed after ~600s of a strain hold (Figure S7B). To further test the sustainability of the response in compression for the M_f ~7.5% composite, it was subjected to a series of cyclic testing conditions. Under a cyclic square wave profile from 5 to 30% strain for 500 cycles, the material's signal in Figure 5A was seen to follow the strain profile accurately. In Figure S8 the material's signal is seen to undergo signal dampening, commonly known as conditioning, with increasing cycle number in

accordance with fatigue theory in nanocomposite strain sensors. The magnitude of the electromechanical signal extrapolated from the first 35 cycles in Figure 5B was shown to scale accordingly with the following power law decay due to the Mullins effect[27]

$$\left(\frac{\Delta R}{R_0}\right)_{R,C} \approx \alpha C^{-B} \quad (4)$$

Where $(\Delta R/R_0)_{R,1}$ is the fractional resistance change range, C is the cycle number, α is a material constant and B is the Basquin exponent. The electromechanical signal of the M_f ~7.5% foam was found to scale as $\sim C^{-0.104}$, with this value for the exponent near the expect value of -0.1 for nanocomposites systems.[27] Unlike previous foam based composite iterations, the composites here displayed a sustainable response without the need of further polymer encapsulant to prevent filler delamination during cycling.[1] We believe that this is due to the natural self-adhering nature uniquely intrinsic to the parent putty material. It can also be noted that though g-putty in itself is highly viscoelastic, no coating ever appears to rub off or to be squeezed out of the foam matrix during any of the cyclic testing. Machine simulated impact tests were used to demonstrate real-time impact monitoring over a range of strain deformations and impact delay times (scheme found in Figure S9). For these tests an unconditioned M_f ~7.5% composite was used to ensure that the effect of conditioning under these more dynamic conditions could be observed. These tests were performed using time delays between cycles of 0, 1 and 5s and for deformations of 0.1, 1 and 10% strain. In all cases the signal again accurately follows the strain profile with very minimal fatigue related changes in electromechanical response (Figure 5C, S10-12). The lack of fatigue effects in the signal of the simulated impact data is consistent with the time dependent recovery of a nanofiller network upon the full realise of applied deformation.[27] In comparison, bulk g-putty under similar testing conditions performed poorly with electromechanical signal being lost after the first 3 cycles (Figure S13).

Impact and Vital Signs Measurements

Previously, g-putty was reported as being a highly accurate impact sensor however, this testing would result in indentations of the putty layer if the impact was too large. With similar sensitivity but superior hysteresis and signal stability, a composite foam of M_f ~7.5% was tested under dynamic impact conditions. Ball bearings of various weights were dropped from several heights to allow for analysis of the material's response over a range of impact energies (E_{mgh}).

As a comparison, bulk g-putty was subjected to similar testing. Plotting the max $\Delta R/R_0$ response for the bulk g-putty and composite foams as a function of E_{mgh}, both datasets are found to overlay one another quite closely and scale similarly with energy according to $E_{mgh} \approx mgh^{0.5}$ (dashed line) in Figure 5D. This exponent has previously been reported to relate to the fractal structure of the graphene network in g-putty[13] and other filler elastomer systems.[28] With their low hysteresis impact measurement capabilities (Figures S9-13) and soft nature, these foam materials would be highly desirable for application as insole replacements in shoes and ideal for the measurement of a wearer's gait. With excellent electromechanical properties comparable to the parent g-putty material, we demonstrated the composite foams to be as equally as effective for vital sign sensing. Holding a M_f ~7.5% composite sample to the carotid artery in a subject's neck allowed for accurate pulse monitoring in real-time (Figure 5E). The noted resistance decay here in the signal was due to the subject being unable to apply even pressure to the foam when holding it to the neck. This however did not affect measurement, as the characteristic initial systolic peak, dicrotic notch and, subsequent diastolic peak of the pulse waveform was reported (inset).

CONCLUSION

G-putty, though is one of the most sensitive and unique electromechanical sensing composite materials, it suffers from plastic deformation at large strains and resistive decay with time. Using a simple foam scaffolding and solution soak method, composites formed from soaking a commercial foam in g-putty inks overcame all the obstacles associated with the bulk material. This scalable method not only presented composite foams that allowed for highly repeatable measurements but also ones with an undiminished sensitivity with respect to the parent material. Applying the above listed properties in application, these highly sensitive smart foams were effectively demonstrated as a real-time bodily impact and vital sign sensors.

EXPERIMENTAL SECTION

G-putty ink was formed using the author's standard method[12] and dispersed into ink form through the bath sonication of the bulk material in chloroform. The preformed stock ink was diluted to create multiple inks of various concentration which then had previously prepared commercial foams soaked in them. The ink saturated foams were then dried to form the composite foams of various loading level that were used in subsequent mechanical and electromechanical testing. Full details of experimental methods and procedures can be found in the Supporting Information.

ACKNOWLEDGMENTS

CSB is grateful for financial support through strategic funding from the University of Sussex. AGK and JNC acknowledge the European Research Council Advanced Grant (FUTURE-PRINT). DPO, JBB and JNC thank the European Union, under grant agreements No. 785219, Graphene Flagship-core 2.

SUPPORTING INFORMATION

The Supporting Information is available online and contains additional experimental details, materials, and methods, including photographs of experimental setup.

- G-putty mechanical, electrical, and hysteresis characterisation, G-putty ink stability characterisation, mechanical and electrical properties of foam composites, signal stability testing, impact testing simulation and signal stability testing.

FIGURES

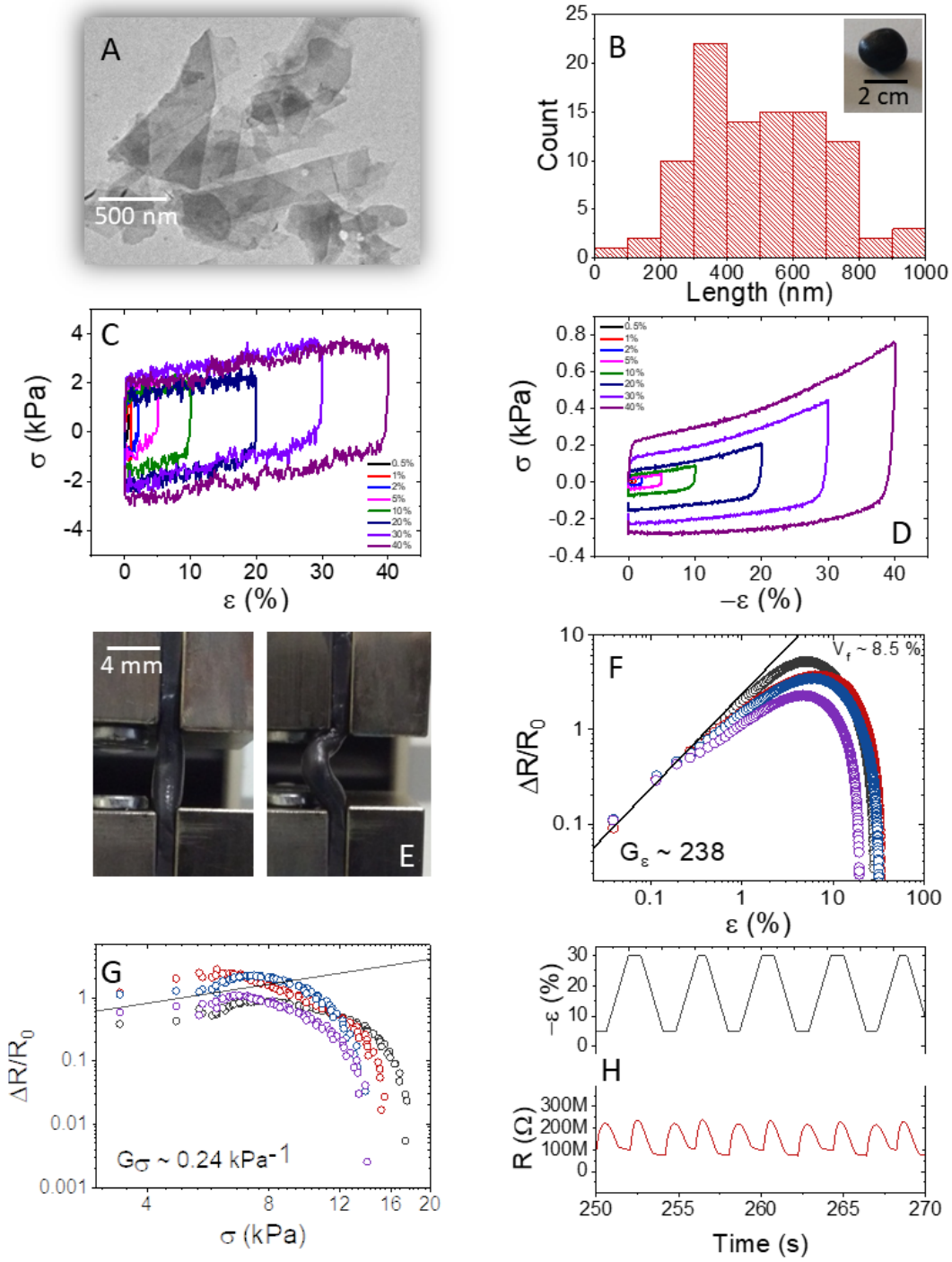

Figure 1: A) Representative TEM image of defect free liquid phase exfoliated graphene nanosheets used to form the stock g-putty composite. B) Histogram showing length distribution of graphene nanosheets recorded from TEM analysis of stock dispersion. Nanosheets are found to have a mean length of ~500 nm. Inset photo shows a picture of the stock g-putty material. C-D) Tensile and compressive hysteresis testing of g-putty showing the large hysteresis loops representative of plastic deformation above 2% strain. E) Photo showing the plastic

deformation of putty after tensile hysteresis testing at holder starting position. F-G) Tensile and compressive electromechanical testing of the stock g-putty. Mean gauge factor of ~238 and ~0.24 kPa^{-1} for tension and compressive are reported. H) Compressive cyclic electromechanical testing of g-putty displaying desync of electrical response (red) with respect to the strain profile (black).

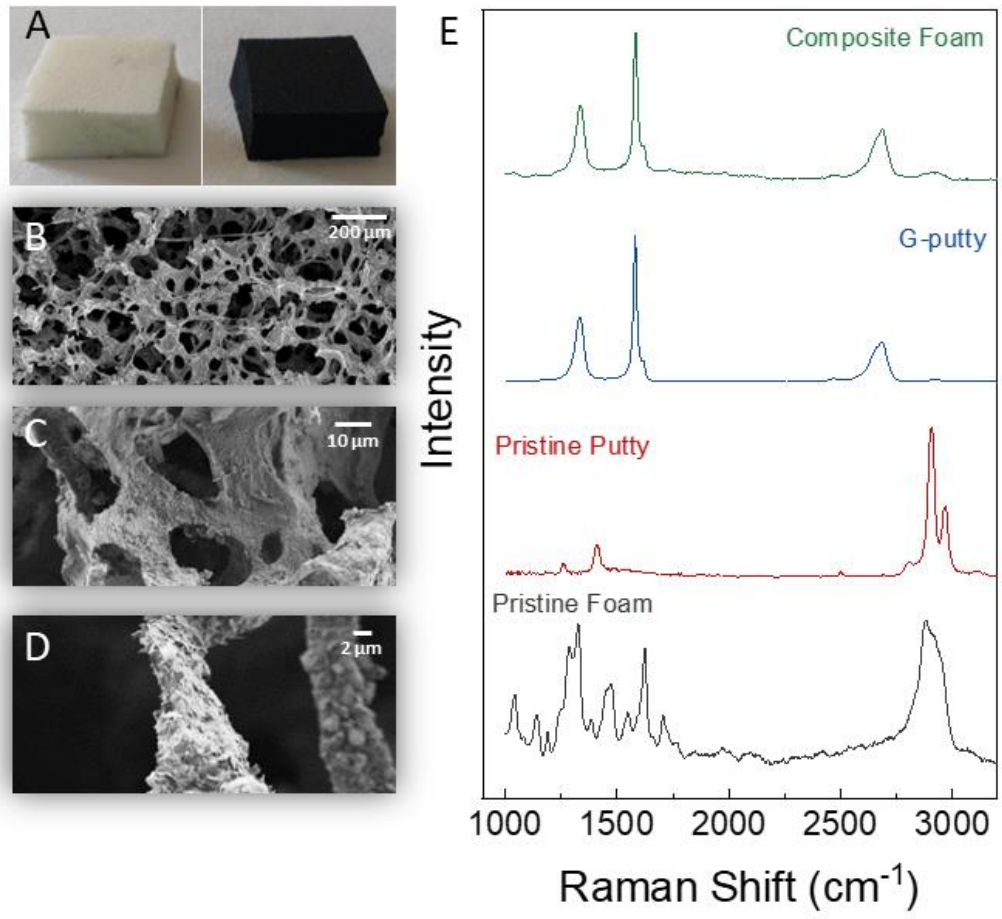

Figure 2: A) Photo of (left) pristine commercial foam and (right) M_f ~ 7.5% g-putty doped foam. B-D) SEM images of the pristine, doped and zoomed view of g-putty coating respectively. E) Raman spectroscopy of (top to bottom) M_f ~7.5% composite foam, g-putty, pristine putty and the pristine commercial foam.

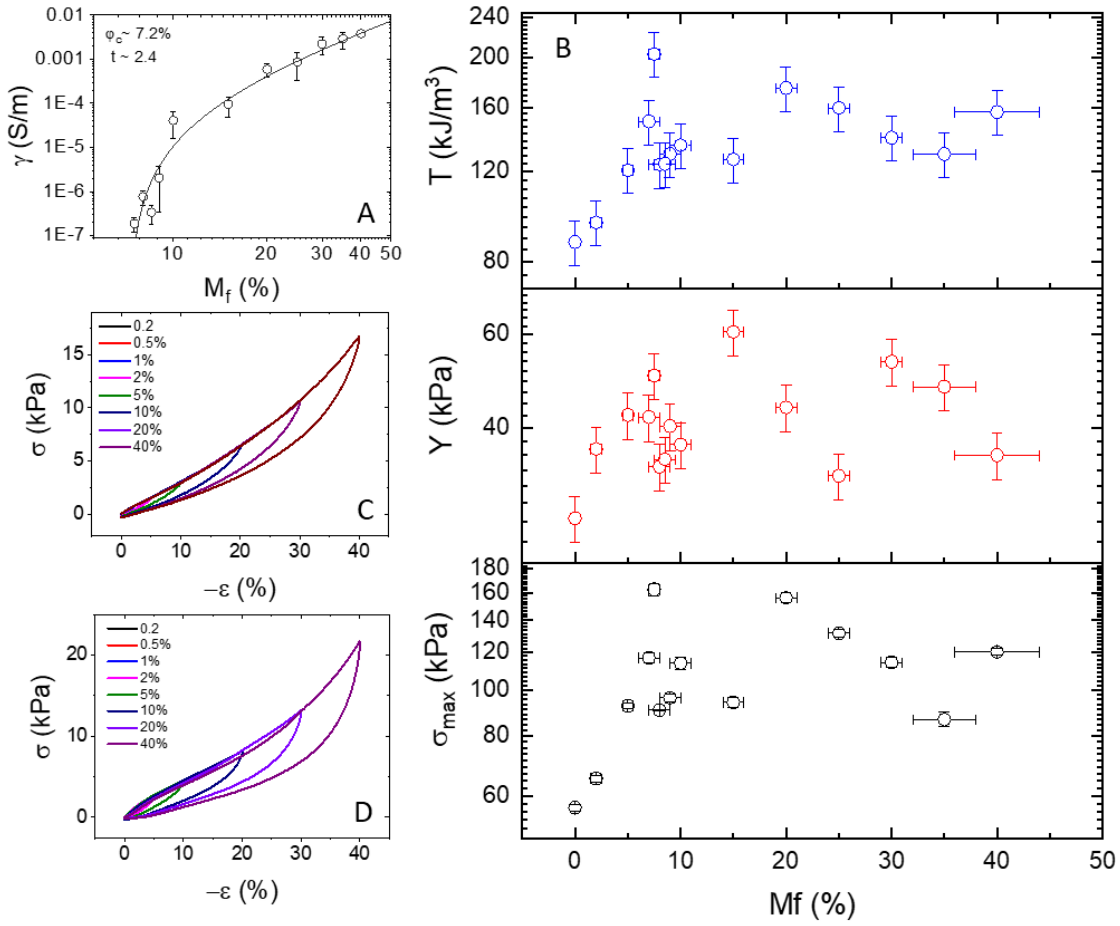

Figure 3: A) Plot of composite electrical conductivity as a function of g-putty loading. Percolation fit of data (solid line, Eq 3) gives a percolation threshold of 7.2% and a percolation exponent of 2.4. B) Toughness (T), Young's Modulus (Y) and Maximum Stress (σ_{max}) plotted as a function of g-putty mass fraction (M_f). Mechanical properties are reported to increase until a saturation point of M_f ~8%, similar to the percolation threshold value. C-D) Compressive hysteresis testing of a pristine and 30% g-putty foam sample respectively.

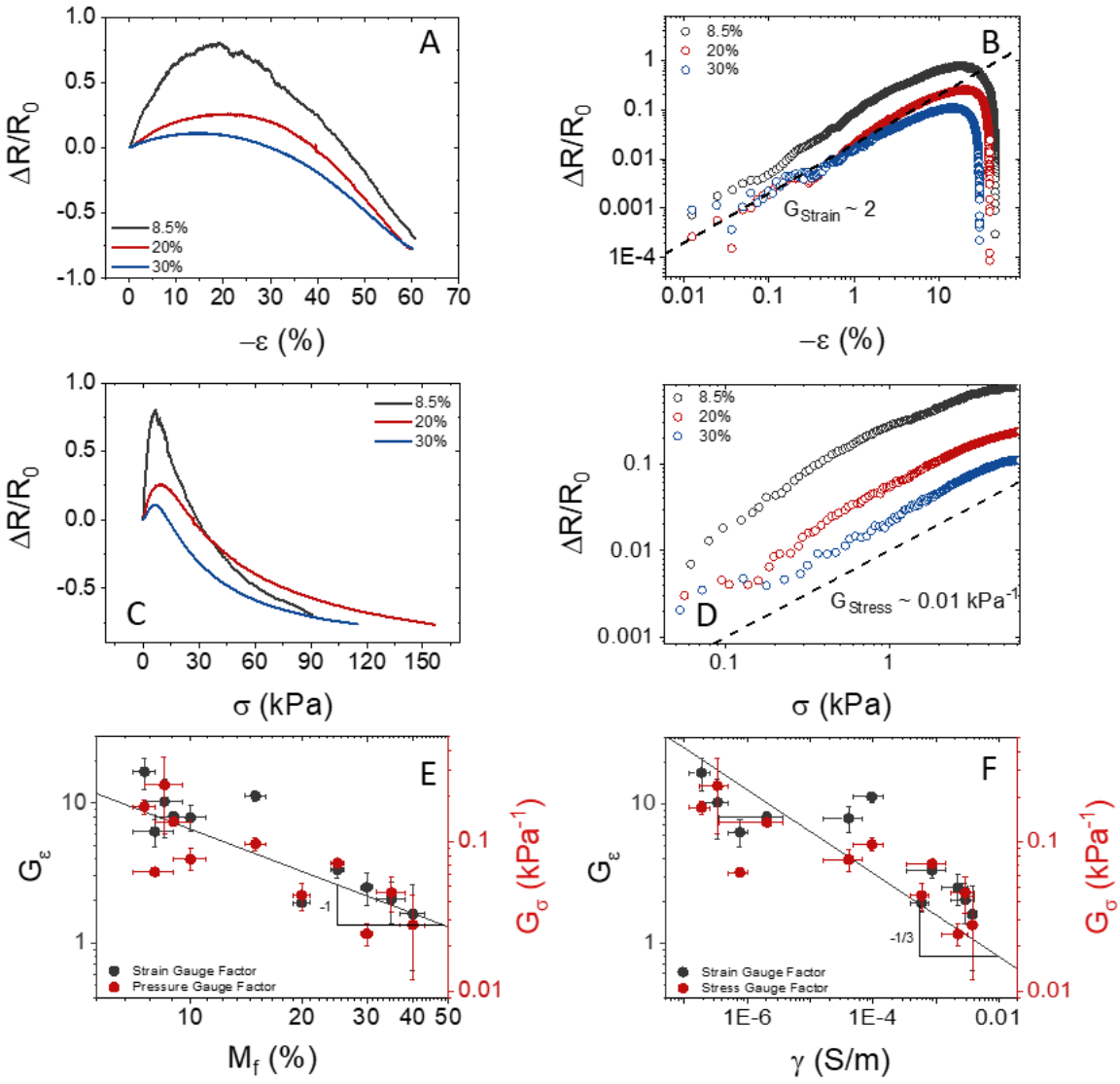

Figure 4: A) Compressive electromechanical testing of a select number of loading levels as a function of strain. B) Log-log plot of A with Eq 1 fitted to the data to represent $G_\varepsilon = 2$ (dashed line). C) Compressive electromechanical testing of a select number of loading levels as a function of stress. D) Log-log plot of C with Eq 2 fitted to the data to represent $G_\sigma = 0.01$ kPa^{-1} (dashed line). E-F) Plots of G_ε and G_σ as a function of M_f and conductivity respectively. The solid lines in E and F represents a $1/M_f$ and $\gamma^{-1/3}$ scaling behaviour respectively.

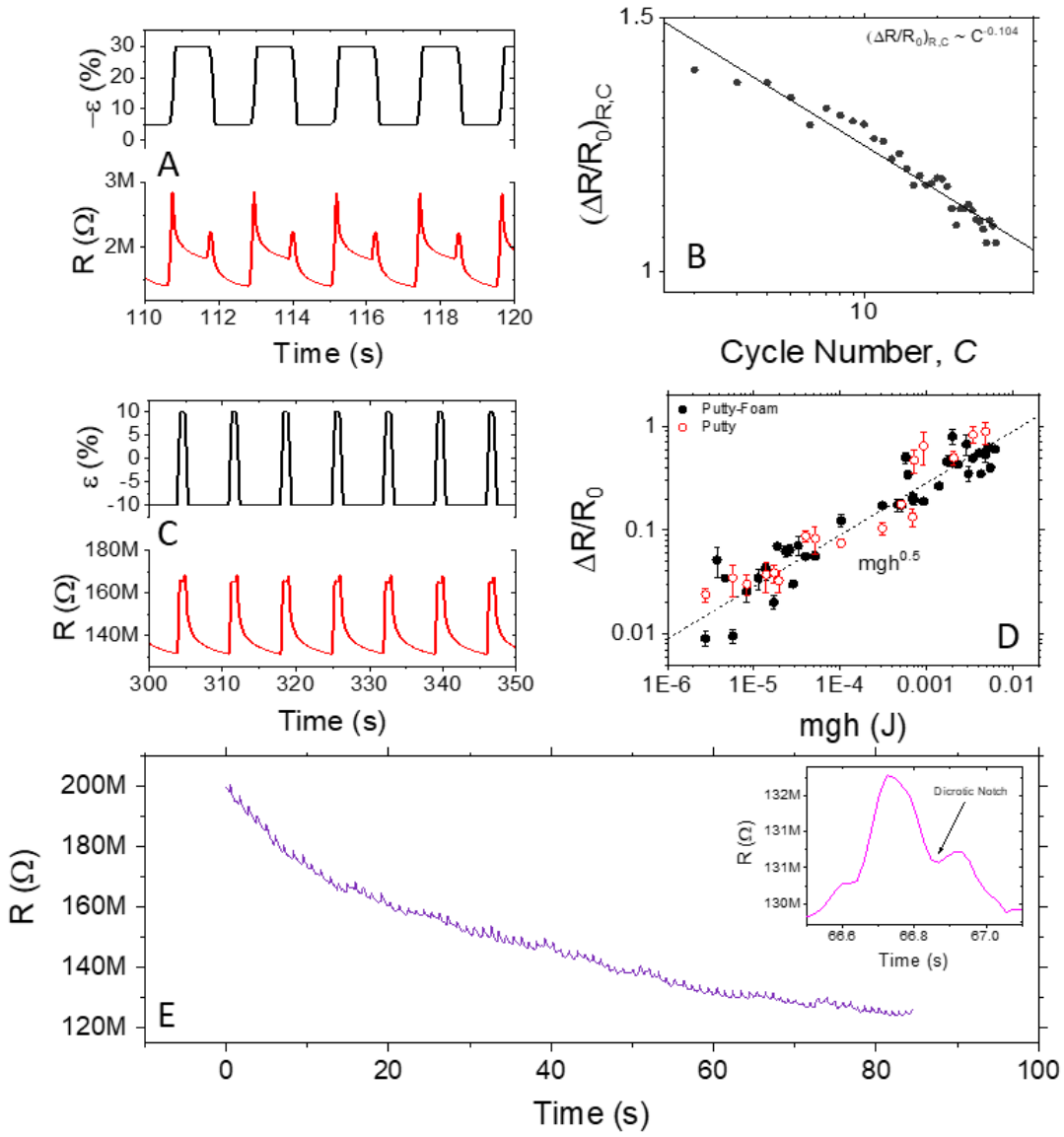

Figure 5: A) Compressive cyclic testing of a M_f ~7.5% composite. B) Fatigue scaling in cyclic data in Figure S8. $(\Delta R/R_0)_{R,1}$, the fractional resistance change range, was found to scale as $\sim C^{-0.104}$. C) Machine assisted impact simulation on 7.5% composite with a 5 second pause and 10% compressive deformation. D) Impact response of a 7.5% composite foam overlaying bulk g-putty's performance. Peak $\Delta R/R_0$ is plotted against potential energy with the dashed line representing the root dependence behaviour of impact potential energy seen for both the foam and bulk material. E) Heart monitoring testing as a function of time (inset) showing characteristic waveform and dicrotic notch.

ToC

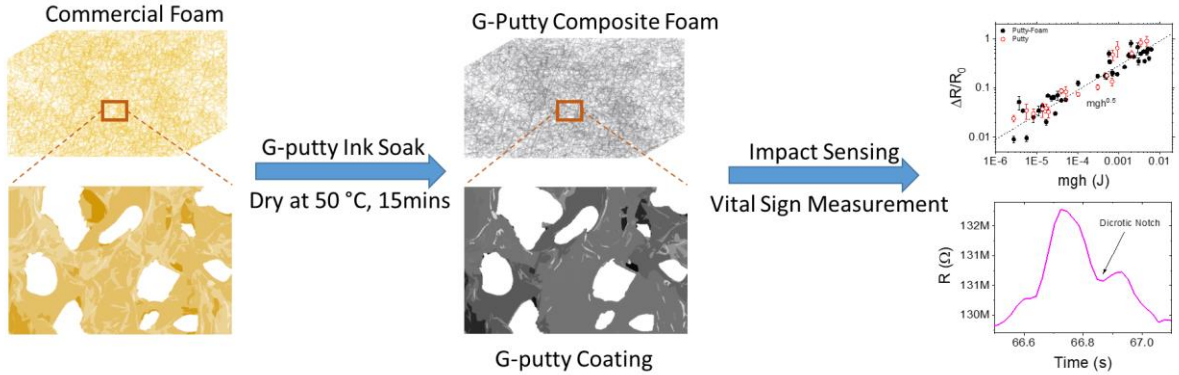
Commercial Foam
G-putty Ink Soak
Dry at 50 °C, 15mins
G-Putty Composite Foam
G-putty Coating
Impact Sensing
Vital Sign Measurement
Putty-Foam
Putty
ΔR/R0
mgh^0.5
mgh (J)
Dicrotic Notch
R (Ω)
Time (s)

REFERENCES

1. Panahi-Sarmad, M.; Noroozi, M.; Abrisham, M.; Eghbalinia, S.; Teimoury, F.; Bahramian, A. R.; Dehghan, P.; Sadri, M.; Goodarzi, V., A Comprehensive Review on Carbon-Based Polymer Nanocomposite Foams as Electromagnetic Interference Shields and Piezoresistive Sensors. *ACS Appl. Electron. Mater.* **2020,** *2* (8), 2318-2350.
2. Ramalingame, R.; Bouhamed, A.; Rajendran, D.; da Veiga Torres, R.; Hu, Z.; Kanoun, O., Highly Sensitive Polymer/Multiwalled Carbon Nanotubes Based Pressure and Strain Sensors for Robotic Applications. *New Trends in Robot Control*, **2020**, 371-382.
3. Afsarimanesh, N.; Nag, A.; Sarkar, S.; Sabet, G. S.; Han, T.; Mukhopadhyay, S. C., A Review on Fabrication, Characterization and Implementation of Wearable Strain Sensors. *Sens. Actuators, A* , **2020,** *315*, 112355.
4. Papageorgiou, D. G.; Kinloch, I. A.; Young, R. J., Graphene/Elastomer Nanocomposites. *Carbon* **2015,** *95*, 460-484.
5. Mehmood, A.; Mubarak, N. M.; Khalid, M.; Walvekar, R.; Abdullah, E. C.; Siddiqui, M. T. H.; Baloch, H. A.; Nizamuddin, S.; Mazari, S., Graphene Based Nanomaterials for Strain Sensor Application—a Review. *J. Environ. Chem. Eng.*, **2020,** *8* (3), 103743.
6. Gong, S.; Cheng, W. L., One-Dimensional Nanomaterials for Soft Electronics. *Adv Electron Mater* **2017,** *3* (3), 1600314.
7. Yao, S.; Swetha, P.; Zhu, Y., Nanomaterial-Enabled Wearable Sensors for Healthcare. *Adv. Healthcare Mater.*, **2018**, 1700889.
8. Oh, J. Y.; Bao, Z., Second Skin Enabled by Advanced Electronics. *Adv Sci*, **2019,** *6* (11), 1900186.
9. Backes, C.; Abdelkader, A. M.; Alonso, C.; Andrieux-Ledier, A.; Arenal, R.; Azpeitia, J.; Balakrishnan, N.; Banszerus, L.; Barjon, J.; Bartali, R.; Bellani, S.; Berger, C.; Berger, R.; Ortega, M. M. B.; Bernard, C.; Beton, P. H.; Beyer, A.; Bianco, A.; Bøggild, P.; Bonaccorso, F.; Barin, G. B.; Botas, C.; Bueno, R. A.; Carriazo, D.; Castellanos-Gomez, A.; Christian, M.; Ciesielski, A.; Ciuk, T.; Cole, M. T.; Coleman, J.; Coletti, C.; Crema, L.; Cun, H.; Dasler, D.; Fazio, D. D.; Díez, N.; Drieschner, S.; Duesberg, G. S.; Fasel, R.; Feng, X.; Fina, A.; Forti, S.; Galiotis, C.; Garberoglio, G.; García, J. M.; Garrido, J. A.; Gibertini, M.; Gölzhäuser, A.; Gómez, J.; Greber, T.; Hauke, F.; Hemmi, A.; Hernandez-Rodriguez, I.; Hirsch, A.; Hodge, S. A.; Huttel, Y.; Jepsen, P. U.; Jimenez, I.; Kaiser, U.; Kaplas, T.; Kim, H.; Kis, A.; Papagelis, K.; Kostarelos, K.; Krajewska, A.; Lee, K.; Li, C.; Lipsanen, H.; Liscio, A.; Lohe, M. R.; Loiseau, A.; Lombardi, L.; López, M. F.; Martin, O.; Martín, C.; Martínez, L.; Martin-Gago, J. A.; Martínez, J. I.; Marzari, N.; Mayoral, Á.; McManus, J.; Melucci, M.; Méndez, J.; Merino, C.; Merino, P.; Meyer, A. P.; Miniussi, E.; Miseikis, V.; Mishra, N.; Morandi, V.; Munuera, C.; Muñoz, R.; Nolan, H.; Ortolani, L.; Ott, A. K.; Palacio, I.; Palermo, V.; Parthenios, J.; Pasternak, I.; Patane, A.; Prato, M.; Prevost, H.; Prudkovskiy, V.; Pugno, N.; Rojo, T.; Rossi, A.; Ruffieux, P.; Samorì, P.; Schué, L.; Setijadi, E.; Seyller, T.; Speranza, G.; Stampfer, C.; Stenger, I.; Strupinski, W.; Svirko, Y.; Taioli, S.; Teo, K. B. K.; Testi, M.; Tomarchio, F.; Tortello, M.; Treossi, E.; Turchanin, A.; Vazquez, E.; Villaro, E.; Whelan, P. R.; Xia, Z.; Yakimova, R.; Yang, S.; Yazdi, G. R.; Yim, C.; Yoon, D.; Zhang, X.; Zhuang, X.; Colombo, L.; Ferrari, A. C.; Garcia-Hernandez, M., Production and Processing of Graphene and Related Materials. *2D Mater.*, **2020,** *7* (2), 022001.
10. Papageorgiou, D. G.; Kinloch, I. A.; Young, R. J., Mechanical Properties of Graphene and Graphene-Based Nanocomposites. *Prog. Mater. Sci.*, **2017,** *90*, 75-127.
11. Boland, C. S., Stumbling through the Research Wilderness, Standard Methods to Shine Light on Electrically Conductive Nanocomposites for Future Healthcare Monitoring. *ACS Nano* **2019,** *13* (12), 13627-13636.

12. O'Driscoll D.P., M. S., Garcia J., Biccai S., Kelly A.G., Barwich S., Moebius M., Boland C.S., Coleman J.N., Printable G-Putty for Frequency and Rate Independent, High Performance Strain Sensors *Small* **2021,** *17* (23), 2006542.
13. Boland, C. S.; Khan, U.; Ryan, G.; Barwich, S.; Charifou, R.; Harvey, A.; Backes, C.; Li, Z.; Ferreira, M. S.; Mobius, M. E.; Young, R. J.; Coleman, J. N., Sensitive Electromechanical Sensors Using Viscoelastic Graphene-Polymer Nanocomposites. *Science* **2016,** *354* (6317), 1257-1260.
14. O'Driscoll, D. P.; Vega-Mayoral, V.; Harley, I.; Boland, C. S.; Coleman, J. N., Optimising Composite Viscosity Leads to High Sensitivity Electromechancial Sensors. *2D Mater.* **2018,** *5* (3), 035042.
15. McCrory, P.; Meeuwisse, W.; Dvorak, J.; Aubry, M.; Bailes, J.; Broglio, S.; Cantu, R. C.; Cassidy, D.; Echemendia, R. J.; Castellani, R. J.; Davis, G. A.; Ellenbogen, R.; Emery, C.; Engebretsen, L.; Feddermann-Demont, N.; Giza, C. C.; Guskiewicz, K. M.; Herring, S.; Iverson, G. L.; Johnston, K. M.; Kissick, J.; Kutcher, J.; Leddy, J. J.; Maddocks, D.; Makdissi, M.; Manley, G. T.; McCrea, M.; Meehan, W. P.; Nagahiro, S.; Patricios, J.; Putukian, M.; Schneider, K. J.; Sills, A.; Tator, C. H.; Turner, M.; Vos, P. E., Consensus Statement on Concussion in Sport—the 5th International Conference on Concussion in Sport Held in Berlin, October 2016. *Br. J. Sports Med.* **2017,** *51* (11), 838-847.
16. 2019 Annual Report, Graphene Flagship. https://graphene-flagship.eu:443/project/annual-reports
17. Hernandez, Y.; Nicolosi, V.; Lotya, M.; Blighe, F. M.; Sun, Z.; De, S.; McGovern, I. T.; Holland, B.; Byrne, M.; Gun'Ko, Y. K.; Boland, J. J.; Niraj, P.; Duesberg, G.; Krishnamurthy, S.; Goodhue, R.; Hutchison, J.; Scardaci, V.; Ferrari, A. C.; Coleman, J. N., High-Yield Production of Graphene by Liquid-Phase Exfoliation of Graphite. *Nat. Nanotechnol.* **2008,** *3* (9), 563-568.
18. Khan, U.; Porwal, H.; O'Neill, A.; Nawaz, K.; May, P.; Coleman, J. N., Solvent-Exfoliated Graphene at Extremely High Concentration. *Langmuir* **2011,** *27* (15), 9077-9082.
19. Boland, C. S.; Khan, U.; Backes, C.; O'Neill, A.; McCauley, J.; Duane, S.; Shanker, R.; Liu, Y.; Jurewicz, I.; Dalton, A. B.; Coleman, J. N., Sensitive, High-Strain, High-Rate Bodily Motion Sensors Based on Graphene-Rubber Composites. *ACS Nano* **2014,** *8* (9), 8819-8830.
20. Boland, C. S.; Khan, U.; Binions, M.; Barwich, S.; Boland, J. B.; Weaire, D.; Coleman, J. N., Graphene-Coated Polymer Foams as Tuneable Impact Sensors. *Nanoscale* **2018,** *10* (11), 5366-5375.
21. Ferrari, A. C.; Basko, D. M., Raman Spectroscopy as a Versatile Tool for Studying the Properties of Graphene. *Nat. Nanotechnol.* **2013,** *8* (4), 235-246.
22. Marsden, A. J.; Papageorgiou, D. G.; Vallés, C.; Liscio, A.; Palermo, V.; Bissett, M. A.; Young, R. J.; Kinloch, I. A., Electrical Percolation in Graphene–Polymer Composites. *2D Mater.* **2018,** *5* (3), 032003.
23. Stankovich, S.; Dikin, D. A.; Dommett, G. H. B.; Kohlhaas, K. M.; Zimney, E. J.; Stach, E. A.; Piner, R. D.; Nguyen, S. T.; Ruoff, R. S., Graphene-Based Composite Materials. *Nature* **2006,** *442* (7100), 282-286.
24. Boland, C. S., Approaching the Limit of Electromechanical Performance in Mixed-Phase Nanocomposites. *ACS Appl. Nano Mater.* **2020**., 11240-11246
25. Samad, Y. A.; Li, Y.; Alhassan, S. M.; Liao, K., Novel Graphene Foam Composite with Adjustable Sensitivity for Sensor Applications. *ACS Appl. Mater. Interfaces* **2015,** *7* (17), 9195-9202.
26. Samad, Y. A.; Li, Y.; Schiffer, A.; Alhassan, S. M.; Liao, K., Graphene Foam Developed with a Novel Two-Step Technique for Low and High Strains and Pressure-Sensing Applications. *Small* **2015,** *11* (20), 2380-2385.

27. Boland, C. S., Quantifying the Contributing Factors toward Signal Fatigue in Nanocomposite Strain Sensors. *ACS Appl. Polym. Mater.* **2020,** *2* (8), 3474-3480.
28. Heinrich, G.; Klüppel, M., Recent Advances in the Theory of Filler Networking in Elastomers. *Filled Elastomers Drug Delivery Systems*, Springer, **2002,** 1-44.